Adaptive repair device concept with shape memory polymer

Wei Zhao[1#], Liwu Liu[1#], Xin Lan[2], Bo Su[3], Jinsong Leng[2], Yanju Liu[1, a*]

1 Department of Astronautical Science and Mechanics, Harbin Institute of Technology (HIT), P.O. Box 301, No. 92 West Dazhi Street, Harbin 150001, People's Republic of China

2 Centre for Composite Materials, Science Park of Harbin Institute of Technology (HIT), P.O. Box 3011, No. 2 YiKuang Street, Harbin 150080, People's Republic of China

3 School of Oral & Dental Sciences, University of Bristol. Lower Maudlin Street, Bristol BS1 2LY, United Kingdom.

[*]*Corresponding author:* Email: yj_liu@hit.edu.cn

Abstract

Shape memory polymer (SMP) is a new kind of intelligent polymer which can be activated by an external stimulus to change and subsequently recover its original shape. Duo to this shape memory effect, SMP can be used in wide range of engineer and bio-medical applications. This paper details an application of SMP on manufacturing of a fracture fixation. The basic properties were characterized by dynamic mechanical analysis (DMA), and the stress relaxation and fatigue were established. A SMP based fracture fixator was designed, analyzed and optimized. Finally, the fixator was fabricated and the fixed effects were verified by experiment in vitro. The performance of SMP based fixator was excellent and proved to be a potential replacement for traditional fracture fixator.

Keywords: *Shape Memory Polymer, Thermoviscoelasticity, Constitutive Theory, Adaptive, Fracture Fixator, Finite Element*

[#] These authors contributed equally to this work.

1. Introduction

Shape memory polymer (SMP) is a new kind of smart material, which can respond to some external environment stimuli and realize active deformation and shape memory effect [[1]-[3]]. Nowadays, there are many stimuli for SMP deformation and recovery, mainly including temperature [4], light [5], electricity [6], magnetic field [7], moisture [8] and solution [9]. Thermally-actuated SMP has been widely applied and achieved great development. Compared with other intelligent materials, SMP possesses advantages of being low cost, low density and having high shape recovery ratios and so on [10-14]. As shown in figure 1, the classic thermo-mechanical cycle for thermal-induced SMP contains four steps. (1) Heat and deform step: fabricate original shape of SMP and heat it above the transition temperature, then apply external force to change the original shape of SMP into a pre-deformed shape; (2) Cool step: keep the deformed shape and cool it below transition temperature; (3) Remove force step: remove the force in low temperature and the deformed shape of SMP is almost maintained; (4) Reheat and recover step: reheat the SMP above the transition temperature and the original shape is recovered.

Due to variable stiffness and shape memory properties, SMP has got wide applications in aerospace [15], textile fabric [16] and biomedicine [17]. Lendlein 2002 [18] et al reported that one SMP served as biodegradable suture, in which the SMP was made into a single fiber wire in the relaxation state to suture the wound. Due to superior biocompatible and biodegradable properties, SMP is increasingly used in biomedical fields. Some researchers have achieved significant success in many bio-medical applications [19-21], such as drug release [22], thrombectomy [23], suture [24], and dental orthopedic operation [25] using various types of SMPs.

Furthermore, combined with proven actuation methods for SMP [26, 27], its application range is broadened greatly.

The majority of recent applications of SMP were focused on small devices. However, some biomedical applications of SMP are of a large scale. Taking fractures for example, the number of traffic and workplace injuries have increased, which has caused an increase in the number of patients with fractured bones. Generally, the tightness of the fixations for fracture treatments, such as plywood and plaster bandage, is difficult to control. As a consequence, it is easy to damage tissue and cause complications. The tightness problem during different treatment stages can be effectively solved when using SMP, due to its variable stiffness and shape memory effects of SMP. Furthermore, due to the advantages of low density, easy deformation, easy assembly and disassembly process and the low cost of SMP materials, the feasibility of SMP for future biomedical applications is very high. Currently, ALL FIT Company [28] has produced plates for fracture to replace plaster bandage. However, plates of thermoplastic material have some drawbacks. It has excellent toughness, but the stiffness is relatively low. Due to this reason, thermoplastic material fixations are not suitable for some body parts where a high fixing effect is required. For some body parts which have a high fixation requirement, their fixing effect is not very satisfactory. Therefore, thermosetting material with higher rigidity is studied for fracture fixator. The material is supplied by Harbin Institute of Technology, and the fabrication of this material has been reported in reference [29]. Using this material, Leng et al. have synthesized SMP composites with multi-shape memory effect, which can selectively actuate to generate complex structures for targeted applications [30]. Additionally, utilizing the variable stiffness property, SMP has been used in smart mandrels to manufacture composite structures with complicated shapes [31].

Inspired by these works, some intelligent novel adaptive devices are designed for fracture fixation, which can achieve different tightness. These fracture fixation devices proposed in this project have characteristics of easy adjustment and high air permeability. Meanwhile, the device can also carry out functional rehabilitation exercise in the rehabilitation process and solve the problem of venous returning easily blocked existing in traditional fracture fixator. Moreover, stiffness of the device can be changed by adding a reinforced phase to satisfy different requirements.

The paper describes the basic material characterization of a chosen SMP which is carried out to ensure that the material has requisite glass-transition temperature, stiffness and strength. Additionally, characterizations of creep, relaxation behavior and thermo-mechanical tests have been performed to establish shape memory behavior. These data are also used to extract material parameters required to carry out simulation studies using ABAQUS commercial Finite Element software. The validity of the simulation is established by comparison with experimental results on coupon level tests. The same simulation technique is then used to study the behavior of some aspects of the fixator designs. Three types of fracture-fixators were considered: for forearm, finger and wrist. In absence of the quantitative data on the requirement of stiffness and strength, the viability of the SMP material and the designed fixators is established only through comparison with the existing fixators such as plaster and the recently introduced thermoplastic ones. Finally, a concept is proposed to achieve an adaptable fixator which would adapt to changes as the swelling of the injured body part decreases over time.

2. Basic mechanical characterization

Obviously, SMP used for biomedical applications must have suitable transition temperature to guarantee enough stiffness at body temperature. Dynamic Mechanical

Analyzer (DMA) is employed to quantify the transition temperature based on the endothermal transition. The basic dynamic mechanical properties, such as tan δ, storage modulus are tested by dynamic mechanical analysis machine. We have synthesized various SMPs with different and tunable T_g and SMP with suitable glass transition temperature and stiffness could be selected for further simulation and experiment based on requirements of biomedical application. For example, the SMP used for fracture fixator must have sufficient strength and stiffness at body temperature, which means the transition temperature (T_g) must be higher than body temperature. However, it must be in acceptable temperature range of human body to avoid scald. Thus, one particular SMP with T_g greater than body temperature was selected for new fixator design.

2.1.1 Dynamic Mechanical Analyzer (DMA)

Considering the limiting temperature that the human body can withstand, the glass transition temperature of selected SMP is about 66.85°C. Dynamic Mechanical Analysis (DMA) is used to study the responding situation of SMP under dynamic loading conditions and different temperatures. The samples used in the DMA test were 2 mm×3 mm×20 mm. Viscoelasticity property of SMP has been characterized by measuring thermodynamic parameters such as storage modulus, tan δ. Figure 2 describes the DMA curve of SMP, where the glass transition temperature is about 66.85°C.

Also, tensile testing, creep testing, relaxation testing and fatigue testing were carried out to obtain the basic mechanical properties, such as elastic modulus, stretch limit and relaxation modulus.

2.1.2 Tensile test of SMP

To characterize the tensile properties of SMP, uniaxial tensile tests under different temperatures have been conducted using Zwick tensile testing machine (figure 3(a)). The test specimen used in this experiment were cut following the standard ASTMD638, Type IV, which were 6 mm wide, 115 mm long, 3 mm thick and of gauge length 25mm. In this procedure, temperatures are arranged from 25°C to 75°C, by steps of 10°C. Figure 3(b) plots the relation between yield and fracture strength and temperature. At room temperature, SMP shows stronger brittle behavior with maximum strain just 1.5%. From the tensile curve it can be observed that SMP undergoes an elastic stage, yield stage and elongation stage before it breaks. SMP experiences three transformation stages in the heating process, i.e. glassy state, viscoelastic state and high-elastic rubber state.

In glassy state the elastic modulus of SMP is approximate 1.9GPa and sharply declines with temperature increasing from 25°C to 50°C, when viscoelastic property is more obvious. After temperature exceeds 60°C, SMP is in high elastic state and has almost no bearing capacity.

The shape fixity is shown in figure 5. From left to right, the extension length of specimens are 5mm，10mm，20mm，30mm，40mm, respectively. Just as shown in figure 5, SMP possesses good deformability and shape memory ability, which can meet the requirements of large deformation of adaptive fracture external fixation device.

2.1.3 Rate-dependent behavior tests

Rate-dependent behavior tests at room temperature (20°C) are shown in figure 6. The test specimens used in this experiment were cut following the standard ASTMD638, Type IV. From the result of the experiment, it can be seen that rate-dependence becomes more obvious with the increase of strain rate. The yield

strength rises as the increase of stain rate. However, the fracture stress shows a great dispersion.

2.1.4 Relaxation test

Maintaining a 1mm deformation of the specimen (ASTMD638, Type IV) for 30 minutes, the relaxation experimental curves are obtained. As shown in figure 7, the stress is about 26MPa at room temperature and reduces to about 21MPa in 30 minutes. SMP exhibits high strength at room temperature, and the viscoelasticity is not obvious until temperature is beyond 35°C. Relaxation modulus decreases rapidly as the temperature increases. When heated to 85°C, the rubbery state polymer can generate high elastic strain.

2.1.5 Cycle loading test

In order to realize external adaptive fracture fixator is reusable, it should undergo several shape memory cycles and loading-unloading situation until failure. In this paper, cyclic loading test has been conducted to study the effect on mechanical property. To meet service conditions of fracture fixator, the cyclic loading experiment has been performed at 30°C and 40°C.

Figure 8(a) is cyclic loading-unloading test at 30°C. The specimen (ASTMD638, Type IV) is cycled between 0.2-1.0 mm at displacement control for 75 cycles. From result of the experiment, it shows that the load decreases to 385N after 75 cycles and tends to stabilize gradually.

The relationship between load and deformation at 40 °C can be shown in figure 8(b). The maximum load declines from the initial 550N to the final 350N as the number of cycles increase. The load decreases sharply in the beginning and tends to stabilize after 30 cycles.

2.3 Shape memory behavior of SMP

The thermo-mechanical cycle test of SMP is measured using tension test specimen (ASTMD638, Type IV) (figure 9). First, the specimen is heated to 90°C and exerted 10mm deformation. In the second stage, deformation is kept and the temperature is lowered to 20°C. Later, load is released. Finally, the specimen is reheated to 90°C with no-load. Now the whole shape memory process is finished. The change of temperature during the cycle period is shown in figure 9(a).

From the deformation-time curve in figure 9(b) it can be seen that the elastic strain recovers quickly at the moment of unloading. Afterwards, memorized strain recovers gradually and turns more and more quickly.

From figure9(c) and figure 9(d) it can be seen that SMP is in super-elastic state when heated to 90°C. Stress is only 0.2MPa in 10mm deformation. During the cooling process, the stress is basically stable before gradually increasing. This is because the volume fraction of freezing phase increases and active phase declines with the temperature decreasing. When it approaches the transition temperature, the stress increases quickly. In this case, the memorized deformation includes elastic deformation which will recover after unloading.

From displacement-temperature curve in figure 9(e) it can be seen that some elastic deformation recover as load release. Afterwards, there is a stage the deformation decreases, which indicated that the effect of thermal expansion phenomenon is taken place. As the temperature reaches 70°C, the recovery of deformation starts to accelerate.

In process of shape memory cycle, variation of stress with strain can be shown in figure 9(f), and stress-strain curve is partially enlarges.

As shown in figure 9(g), variation of stress, strain with temperature and the relationship among parameters above can be shown clearly.

3. Simulation of SMP

3.1 Constitutive modeling of SMP

In this paper, the relaxation curves under different temperatures are transformed along the time axis based on the time-temperature equivalent principle introduced by Tobolsky and Catsiff [32]. According to the principles of the time-temperatures superposition principle, both time and temperature are equivalent. In this work, the WLF [33] (proposed by Williams, Landel and Ferry) equation is used to describe time-temperature equivalence, which can be described as:

$$loga_T = \frac{-c_1(T-T_0)}{c_2+(T-T_0)} \tag{1}$$

The equation describe the equivalent isothermal difference between two experiments with the same strain rate, which T_0 and T represent the experiment at T_g and an elevated temperature. C_1, C_2 are conversion constants of WLF equation.

Then the master curve at 50°C is obtained. The relationship between logE(t) and logt can be obtained from relaxation curves (figure 10). Variation with *logt*, *logE(t)* can be approximately treated as straight lines and can be expressed by regression line as:

$$logE(t)=A+Blogt \tag{2}$$

In this paper, the combined model of multi-types is adopted to simulate the mechanical behavior of thermo-viscoelasticity and large deformation. The Boltzmann superposition principle (BSP) provides an accurate model for the polymer's viscoelastic mechanical response [34, 35]. The corresponding constitutive equation is described as:

$$\sigma(t)=\int_{-\infty}^{t} E(t-\tau)\frac{\partial}{\partial\tau}\varepsilon(\tau)d\tau \tag{3}$$

Where *E(t)* is the relaxation function.

For relaxation test of SMP, strain can be described as,

$$\varepsilon(t)=\varepsilon_0 h(t) \tag{4}$$

Where $h(t)$ is Heaviside unit step function; ε_0 represents strain amplitude. The relaxation function can be expressed as

$$E(t)=0, \qquad t<0 \tag{5}$$

$$E(t)=\sigma(t)/\varepsilon_0, \qquad t\geq 0 \tag{6}$$

Applying step strain to specimen, stress relaxation modulus is described as:

$$E(t)=E_e+\sum_{i=1}^{n} E_i \exp\left(-\frac{t}{\tau_i}\right) \tag{7}$$

Where τ_i is relaxation time and can be expressed as $\tau_i=\eta_i/E_i$. When $t\rightarrow 0$, the equation can be illustrated as:

$$E_0=E_e+\sum_{i=1}^{n} \exp\left(-\frac{t}{\tau_i}\right) \tag{8}$$

3.2 Simulation of shape memory effect

The shape memory effect of specimen (ASTM D638, type IV) was simulated with a three dimensional model. Only the middle part of the specimen was modeled, and the dimension of the modeled part was 65mm. The specimen was modeled with ABAQUS C3D8R elements, and the number of elements was 1170. The model is partitioned with hexahedron mesh and simple tensile force is applied at both ends as shown in figure 11. Related material properties are listed in table 1. The coefficient C1 and C2 were assumed to be constant during each step. In this model, τ and g were viscoelastic parameters; E represented elastic parameters; a represented thermal expansion coefficient.

As indicated above, the explicit method available in ABAQUS is employed to simulate the shape memory cycle. The analysis step of simulation is same with the

process of experiment. After processing all time steps, the shape memory cycle of total time is represented.

Using the model parameters in table1, the results from simulations are compared to the experimental results. Figure 11(b) is the contrast of temperature vs. time. Stress vs. temperature is represented in figure 11(c). The variation trends of two curves closely match however there is a little difference. The reason for differences is that cooling rate is constant in ABAQUS whereas it is not constant in actual situation, which indicates the variation of stresses closely related to temperature. Figure 11(d) is the results of stress vs. strain. From the result curve figure 11(d) it can be seen that the variation trends between simulation and experiment are similar and maximum stress at each case about 5.8MPa. Figure 11(e) shows variation of stress with time. The simulation results show a little difference in loading process, but the average trend is similar. In the simulated results of figure 11(c) and (e), there is a change in slope of the stress vs. time and temperature vs. stress, since the accuracy of load measurement of machine cupping is limited. So there are some deviations between the obtained viscoelastic parameters of g3 and g4 by fitting the experimental data.

The model parameters used in this paper are obtained by fitting experimental data. There are two major error resources while fitting data: i.e. the limited precision of load cell of test machine; and the errors caused by fitting experimental data. In this paper, the model parameters are partly obtained by fitting the relaxation data. There are some uncompromised shortcomings inherited in present analysis. One major cause is at higher temperature than glass transition temperature, the specimen loses its loading capacity, gradually. Also due to the finite precision of load-control machine cupping, the relaxation data in high temperature have some deviation with relaxation data in low temperature. Besides, the parameters of WLF equation are fitting by least

square method, which causes further deviation. Due to these reasons, the viscoelastic parameters g3 and g4 which were deduced from curve fitting into experiment data, contains some errors.

4. Design and test of fracture fixator

Generally, it is difficult to control tightness of fracture fixator and thus, it is easy to cause oppressive organization, allergic symptoms and the fracture displacement. Based on variable stiffness properties, good deformation and shape recovery ability of SMP, new intelligent adaptive devices for fracture fixation were developed and investigated. To evaluate suitability of SMP for a fixator, the bending property of SMP with circular holes is compared with other products (figure 12). The specimen used in this test are all are 30 mm wide, 50 mm long and of span 30mm. The thickness of SMP and the thermoplastic material are 3mm, and the gypsum plate is 7mm. The obtained flexural modulus of SMP plate, the product of thermoplastic material and gypsum are respectively 421MPa, 122MPa and 394MPa. Experimental results show that the flexural modulus of SMP plate with circular holes is significantly higher than the product of thermoplastic material but closer to the modulus of gypsum. Thus, these SMP plates are stiffer and stronger than the product of thermoplastic material and traditional gypsum plate.

4.1 Fracture fixator for forearm

A forearm of a volunteer is selected as the experimentation, and then its size and shape is determined. The fixed plate circles around the forearm exactly, and target is modeled easily with the help of CATIA 3D modeling software. Meanwhile, ventilation holes are provided in the fixing plate is to increase the gas permeability. To assure adequate stiffness, the fixed plate has relevant requirements for the location and size of holes, which the horizontal and vertical distance between the ventilation

holes is 5 mm and the hole-circle diameter is 1mm. The above results indicate that the fixed plate with circular holes has better stiffness at room temperature.

4.1.1 Tension test for fracture fixator scale model of forearm

To explore the effect of holes shapes on fixed plate stiffness and satisfy the aesthetic needs of patients with their different styles, two kind of fixed plate are designed with square holes and circular holes respectively. For convenience, the mechanical properties of the fixator have been tested by scale 1:5 fracture fixator. The proportion between the scale model and the original device is 1:5. The tensile tests at 60°C of scale fixator are shown in figure 13. From tension curves we can see that the two kinds of structures almost have the same limit load, and the elongation percentage is above 80%. From the tensile curves (figure 13(a)), we can see that there is a yielding phase during the deformation. As seen in figure 13(b) of circular holes scale model, the fracture first occurs in middle of the structure. Afterwards the load decreases gradually until break.

4.1.2 Restoring force test for fracture fixator scale model of forearm

The recovery force test of scale structure has been conducted. As shown in the figure 14 tensile stress gradually turn to compressive stress during temperature-rise period. The load increases to 35N at the beginning, then it decreases to 0 and increases reversely to 32N. The reason why there exists compressive stress is that thermal expansion plays a leading role at the beginning of heating stage.

4.1.3 Creep test for fracture fixator scale model of forearm

The creep experiment of scale structure has been conducted. The fixed performance is characterized by creep curves. At 60°C, the creep property under load of 600N and 700N is compared in detail. As shown in figure 15 the final deformation is about 0.8mm 1800 seconds after loading, which indicates that the structure still has

high creep-resistance at ambient temperature. So it can be concluded that the structure is suitable for fracture fixation under body temperature.

4.1.4 Three-point bending test for fracture fixator scale model of forearm

Three-point bending tests at 30°C, 40°C, 50°C have been conducted (figure 16), in order to explore SMP fixator's flexural stiffness. The sample used in this test is the scale structures, which are 30 mm wide, 50 mm long and 3 mm thick and of span 30mm. As shown in figure 16(a), the flexural has decreased while changing the temperature from 30°C to 40°C, and it can be conclude that support force is enough around body temperature.

When temperature is 50°C or even higher, the structure can experience large deformation, making sure it can be taken down successfully. Though the scaled model has higher stiffness at 30°C, SMP is tougher at 40°C so that the fracture deformation of the scale model is larger when the temperature is 40°C. And the stiffness of the scale model at 40°C is high enough to make the fracture load higher than that at 30°C.

The result of three-point bending test at 50°C is illustrated in figure 16(b). At this temperature, the limit load is about 80N. After the load reaching 80N, the structure continues to deform until it loses loading capacity.

4.1.5 Restoring force test of three-point bending of forearm fracture fixator

The three-point bending has been conducted for investigation of restoring force. As shown in figure 17 the restoring force increases quickly in the initial phase. After 200 seconds the speed tends to slow down and in about 300 seconds the load reaches the maximum value of 16N. Then the load decreases gradually until the structure loses the bearing capacity.

4.1.6 Simulation of fracture fixator scale model

The shape memory effect of fracture fixator scale model is simulated with a three dimensional model. The fixator is modeled using commercial Finite Element software ABAQUS. General purpose C3D8R solid elements were used to mesh the sample and the number of elements is 10176 (figure 18). The proportion between the scale model and the primary structure is 1:5. An initial deformation of 5mm was applied to the scale model and a stress contours are shown in figure 19. From stress map we can see that the maximum stress is about 2.36MPa in the middle of structure.

The stress contour plots of final state of each analysis step are shown in figure 20. The variation of stress with time has been shown in figure 21.

As seen in figure 22, the contour of displacement is the last state of each analysis step. The maximum deformation turns from the initial 5mm to 4.448mm in the third step for the elastic strain recovery. The variation of deformation with time in the process of shape memory cycle is shown in figure 23.

The fixator for arm is verified experimentally (Figure 24). Figure 24(a) shows the designed structure of fixator for forearm. As shown in figure 24(b), the fixed effect is satisfactory. The prototype of fixator should be dipped into water higher than glass transition temperature before using it. After the structure becomes soft, it is dried out, and then fixed into an arm. When the structure is cooled below glass transition temperature, the shape is preserved after releasing the outside pressure. During the fixed period, this structure exhibited good gas permeability and easy installation. It has provided an adequate support for arm and has shown a good fixing efficiency.

4.2 The fixator of middle finger based on SMP

For second prototype testing-a middle finger of the volunteer was selected, and its size and shape was measured. The fixed plate circled around the finger exactly, and the target is modeled easily with the help of CATIA modeling software. To verify the fixation property of the fixator, vitro test has been conducted (figure 25). Figure 25(a) is the designed structure for middle finger. The experimental results show that it has enough stiffness at body temperature which can offer sufficient support force.

The fixing state of middle finger fixator based on SMP is shown in figure 25(b). It is similar to fixator for arm before using; it should be dipped into water higher than glass transition temperature. After the structure becomes soft, it is dried out. At the temperature below glass transition the shape is memorized. Subsequently, overlapping tapes were used to fix the shape. When disassembling it, the structure was reheated. Repeating the above steps, the second fracture fixation can be finished.

Two kinds of SMP fixity devices for fractures are designed to resolve important problems such as disassembly after the fracture healing stage. The traditional fixator needs to break the plaster for fracture, which can easily cause harm to the patient. These new structures significantly simplify the disassemble process, which in turn significantly decrease the chances of harm to the patient

4.3 Fixator for wrist based on SMP

A fixator of wrist based on SMP was designed to fit a volunteer's wrist was measured. Figure 26 is the designed structure and fixation method, respectively. The fixator is still 3mm thick. Due to the shape memory effect, it is convenient for preservation, saving a lot of room. It can not only be used as a fracture fixator, but also a wrister. Besides, if the motion is restricted, the shape of the fixator could be changed arbitrarily by applying thermo stimulus.

4.4 Adaptive fracture fixator

Furthermore, an adaptive repair device concept is proposed based on adjustable stiffness. Like the previous, the forearm of a volunteer is selected for the experiment, and then its size and shape was determined. On the basis of forearm size, a tube-shape structure with a diameter slightly larger than the forearm is manufactured.

Generally, injured limb is accompanied with swelling. During the treatment, the swelling goes down gradually as fracture heals, which results in loosing of traditional fracture fixator. However, the adaptive repair device concept proposed in this paper can accomplish real-time adaption of the tightness according to the configuration of the injured limb. Therefore, the fixator has property of self-adaptability. When the injured limb becomes loose, applying thermo stimulus to fracture fixator, it can readjust to and remain the best fixed state.

As shown in figure 27, the fixator is firstly expanded to a certain state with the cross-section diameter larger than the “injured part”. The swelling state of “injured part” is simulated by gasbag. By releasing gas, it simulates its detumescence. Meanwhile, stimulating SMP fracture fixator continuously readjusts its real-time state. Due to the shape memory effect, the fixator remains in its best fixed state.

Different from flat fixator proposed above, this kind of fixation device focus on air permeability and shape fixity ability during fracture healing stage. The outstanding advantages of the fixator are light quality, good permeability and adjustable stiffness. Certainly, to actualize this function it may be necessary to combine with other techniques, such as force chip sensing tightness and temperature sensor sensing temperature.

5. Conclusion

In this paper, the basic mechanical properties of SMP are characterized by dynamic mechanical analysis (DMA) test and stress relaxation as well as cycle loading experiments. Based on the characteristics of material, the glass transition temperature of SMP is selected, which can satisfy various conditions of the medical field. Referring to the existing fracture fixation devices, the design scheme of intelligent adaptive fracture fixation device is proposed. Then simulation of shape memory process is conducted. Thus, a basis is provided for the development of fracture fixation device. According to the finite element analysis and optimizing design scheme, the intelligent adaptive device is manufactured for fracture fixation. Then the fixed effect and adaptive response of fixator is verified by experiments in vitro, which reflects the operability and the superior performance of the fixator. The study provides a facile engineered strategy for design of fracture fixator.

Acknowledgement

This work is supported by the National Natural Science Foundation of China (Grant No.11225211).

Reference

[1]. Behl M and Lendlein A 2007 Shape-memory polymers Materials Today 10 20-28

[2]. Sinha R and Jarali C 2011 Raja S. Modelling the thermomechanical behaviour of shape memory polymer materials. Indian J. Phys. Eng. Mat Sci. 18 15-23

[3]. Leng J, Lan X, Liu Y and Du S 2011 Shape-memory polymers and their composites:Stimulus methods and applications Prog. Mater. Sci. 56 1077-1135

[4]. Yu K, Ge Q, Qi H 2014 Reduced time as a unified parameter determining fixity and free recovery of shape memory polymers Nat. Commun. 5 3066

[5]. Leng J, Zhang D, Liu Y, Yu K and Lan X 2010 Study on the activation of styrene-based shape memory polymer by medium-infrared laser light Appl. Phys. Lett. 96 111905

[6]. Liu Y, Lv H, Lan X, Leng J and Du S 2009 Review of electro-active shape memory polymer composite Compos. Sci. Technol. 69 2064-2068

[7]. Yu K, Westbrook K, Kao P, Leng J and Qi H 2013 Design consideration for shape memory composites with magnetic particles. J. Compos. Mater. 47 51-63

[8]. Yang B, Min H, Li C and Hoe C 2005 Effects of moisture on the glass transition temperature of polyurethane shape memory polymer filled with nano-carbon powder Eur. Polym. J. 41 1123-8

[9]. Huang W, Yang B, An L, Li C and Chan Y 2005 Water-driven programmable polyurethane shape memory polymer: demonstration and mechanism Appl. Phys. Lett. 86 114105

[10]. Tobushi H, Hashimoto T, Ito N, Hayashi S and Yamada E 1998 Shape fixity and shape recovery in a film of shape memory polymer of polyurethane series J. Intell. Mater. Syst. Struct. 9 127-36

[11]. Lu H, Liu Y, Gou J, Leng J and Du S 2010 Synergistic effect of carbon nanofiber and carbon nanopaper on shape memory polymer composite Appl. Phys. Lett. 96 084102

[12]. Meng Q and Hu J 2009 A review of shape memory polymer composites and blends Compos. Part A-Appl S 40 1661-72

[13]. Xie T 2011 Recent advances in polymer shape memory Polymer 52 4985-5000

[14]. Hu J, Zhu Y, Huang H and Lu J 2012 Recent advances in shape-memory polymers: structure, mechanism, functionality, modeling and applications Prog. Polym. Sci. 37 1720-63

[15]. Robert Bogue 2009 Shape-memory materials: a review of technology and applications Assembly Automation 29 214-219

[16]. Jinlian Hu and Shaojun Chen 2010 A review of actively moving polymers in textile applications J. Mater. Chem. 20 3346-3355

[17]. Yakacki C M and Gall K 2010 Shape memory polymers for biomedical applications [M]. //Shape-memory polymers. Springer Berlin Heidelberg 147-175

[18]. Lendlein A, Behl M, Hiebl B and Wischke1 C 2010 Shape-memory polymers as a technology platform for biomedical applications. Expert Rev. Med. Devic. 7 357-379

[19]. Cabanlit M, Maitland D, Wilson T, Simon S, Wun T, Gershwin E and Water. Polyurethane Shape-Memory Polymers Demonstrate Functional Biocompatibility In Vitro Macromol. Biosci. 7 48-55

[20]. Yakacki C, Shandas R, Safranski D, Ortega A, Sassaman K and Gall K 2008 Strong, Tailored, Biocompatible Shape-Memory Polymer Networks. Adv. Funct. Mater. 18 2428-2435

[21]. Serrano M and Ameer G 2012 Recent Insights Into the Biomedical Applications of Shape-memory Polymers. Macromol. Biosci. 12 1156-1171

[22]. Wischke C, Neffe A, Steuerand S and Lendlein A 2009 Evaluation of a degradable shape-memory polymer network as matrix for controlled drug release J. Control. Release 138 243-250

[23]. Small W, Wilson S, Benett W, Loge J and Maitland J 2005 Laser-activated shape memory polymer intravascular thrombectomy device Opt. Express. 13 8204-8213

[24]. Huang W, Songb C, Fuc Y, Wanga C, Zhaoa Y, Purnawalia H, Lud H, Tanga C, Dinga Z and Zhang J 2013 Shaping tissue with shape memory materials. Adv. Drug. Deliv. Rev. 65 515-535

[25]. Jung Y and Cho J 2010 Application of shape memory polyurethane in orthodontic J Mater Sci-Mater M 21 2881-2886

[26]. Wang W, Lu H, Liu Y and Leng J 2014 Sodium dodecyl sulfate/epoxy composite: water-induced shape memory effect and its mechanism. J. Mater. Chem. 2 5441-5449

[27]. Lu H, Gou J, Leng J and Du S 2011 Magnetically aligned carbon nanotube in nanopaper enabled shape-memory nanocomposite for high speed electrical actuation. Appl. Phys. Lett. 98 174105

[28]. http://www.allfit.com.cn/product_show.asp?id=59

[29]. Zhang D, Liu Y, Yu K and Leng J 2011 Influence of cross-linking agent on thermomechanical properties and shape memory effect of styrene shape memory polymer. J Intel Mat. Syst. Str. 22(18) 2147-2154

[30]. Li W, Liu Y and Leng J 2015 Selectively actuated multi-shape memory effect of a polymer multicomposite J. Mater. Chem. 3(48) 24532-24539

[31]. Du H, Liu L, Leng J, Peng H, Scarpa F and Liu Y 2015 Shape memory polymer S-shaped mandrel for composite air duct manufacturing Compos. Struct. 133 930-938

[32]. Tobolsky A and Catsiff E 1956 Elastoviscous properties of polyisobutylene (and other Amorphous Polymers) from stress-relaxation studies. IX. A Summary of Results J. Polym. Sci. 19 111-121

[33]. Williams M, Landel R and Ferry J 1955 The temperature dependence of relaxation mechanisms in amorphous polymers and other glass-forming liquids J. Am. Chem. Soc. 77 3701-3707

[34]. Mas E, Clements B, Blumenthal W, Cady C, Gray G and Liu C 2002 A viscoelastic model for PBX binders AIP Conf. Proc. 620 661-664

[35]. Clements B and Mas E 2001 Dynamic mechanical behavior of filled polymers. I. Theoretical Developments Appl. Phys. Lett. 90 5522-5534

Figure Caption

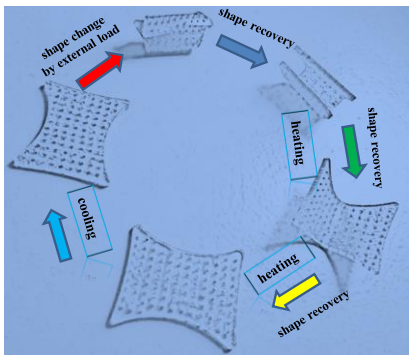

Figure 1 Classic thermomechanical cycle of SMP

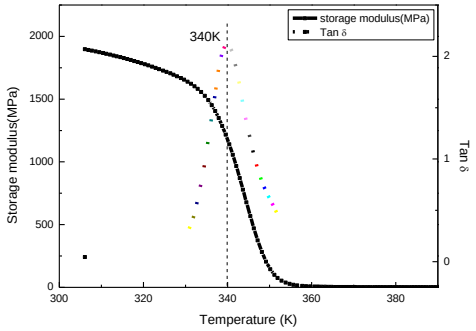

Figure 2 Dynamic mechanical analysis of the SMP

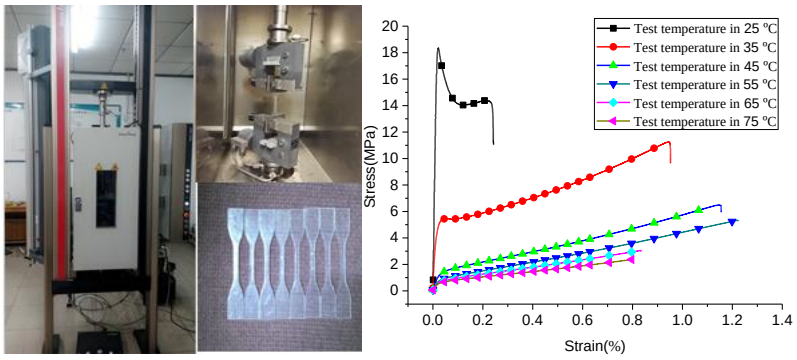

(a) (b)

Figure 3 Tensile test of SMP under different temperatures (a) Zwick tensile test machine (b) Stress-strain curves (Deformation rate: 2mm/min)

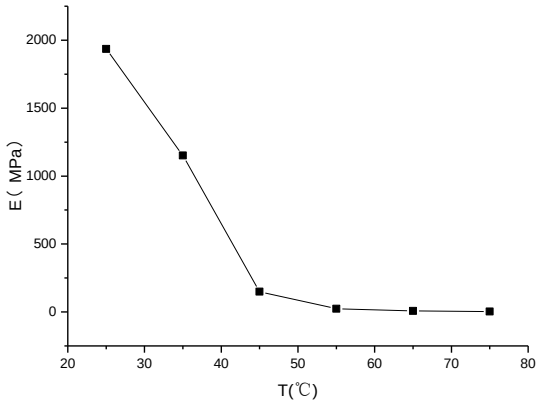

Figure 4 Elasticity modulus of SMP under different temperatures

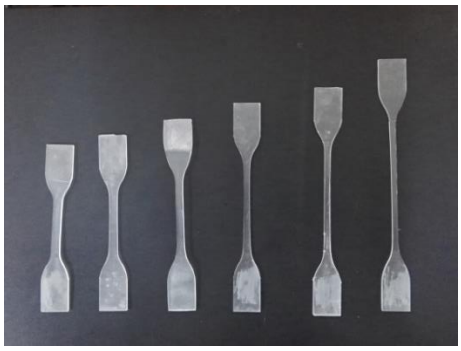

Figure 5 Shape fixity of SMP

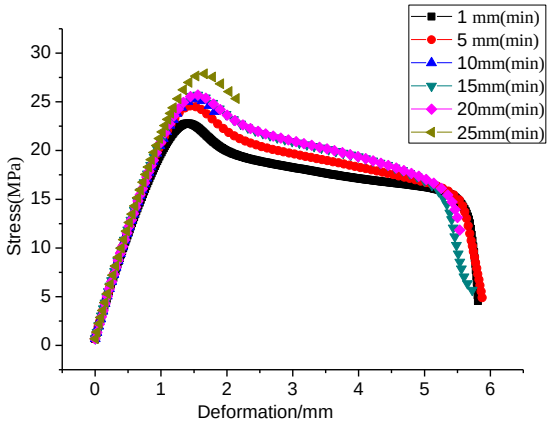

Figure 6 Rate-dependent behavior test curves of SMP (at 20℃)

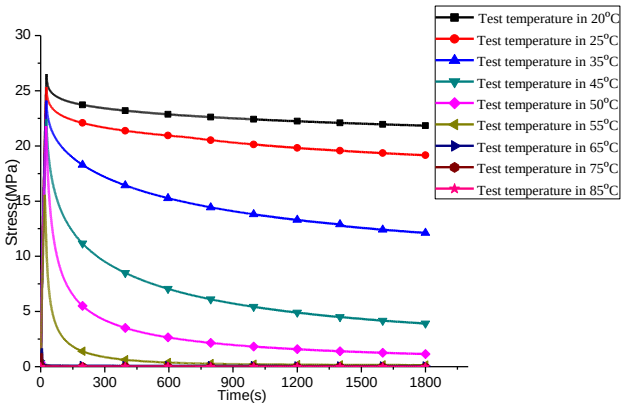

Figure 7 Relaxation test curves under different test temperatures

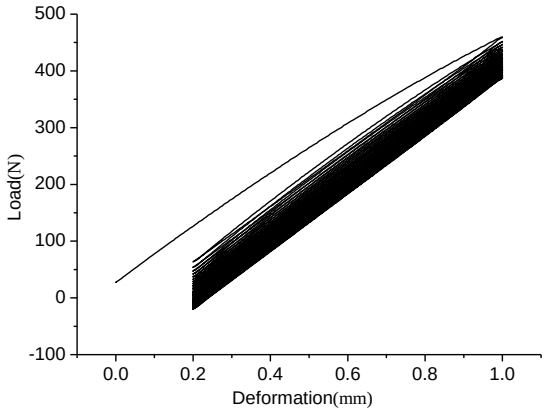

(a) Cycle test at 30°C (Deformation rate: 2mm/min)

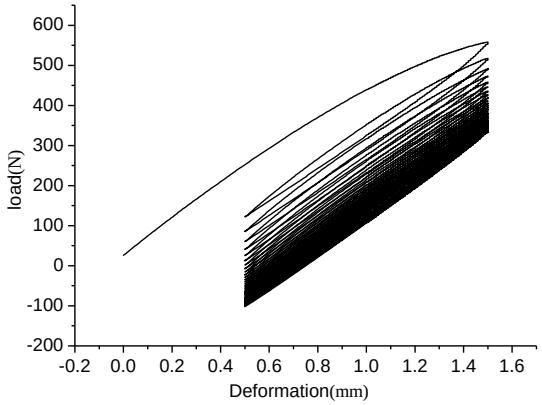

(b) Cycle test at 40°C (Deformation rate: 2mm/min)

Figure 8 Load-deformation curves

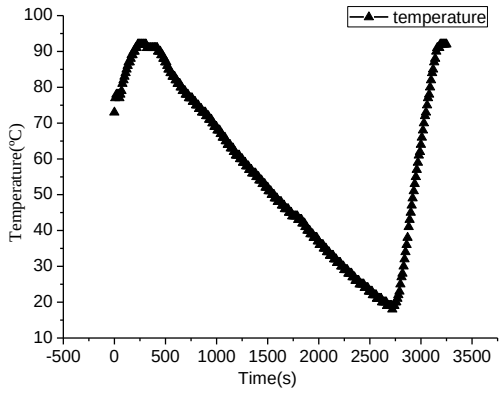

(a) Temperature-time curve

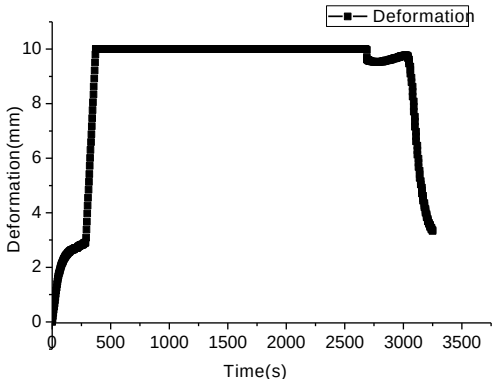

(b) Deformation-time curve

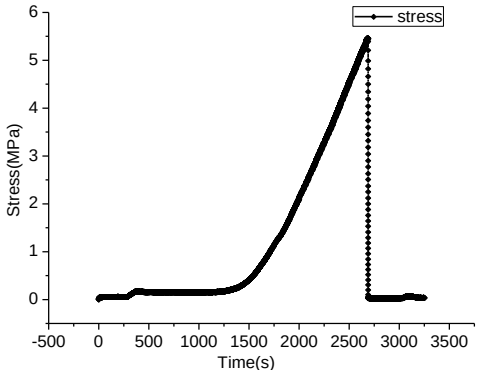

(c) Stress-time curve

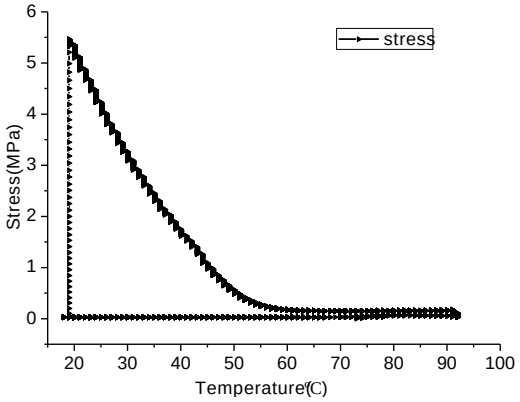

(d) Stress-temperature curve

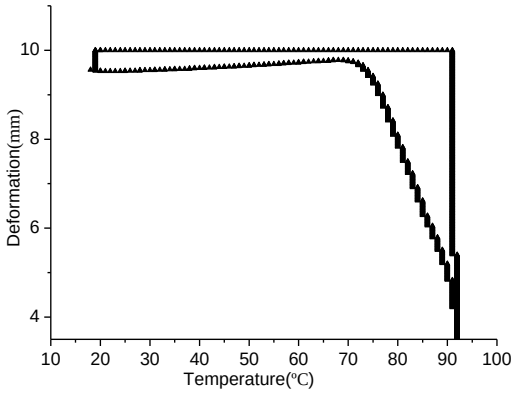

(e) Deformation-temperature curve

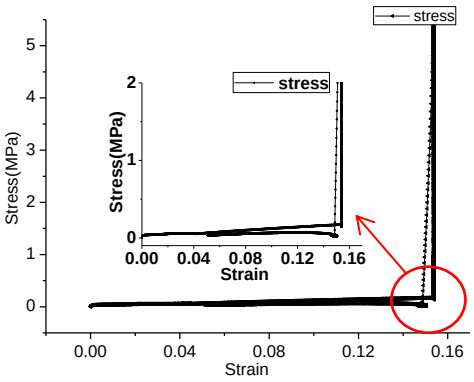

(f) Stress-strain curve and partial enlarges

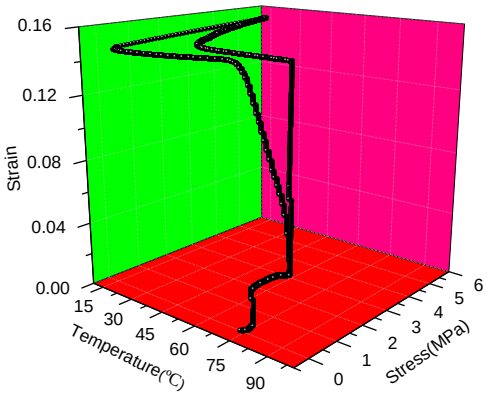

(g) Stress-strain-temperature curve

Figure 9 Thermo-mechanical cycle test of SMP

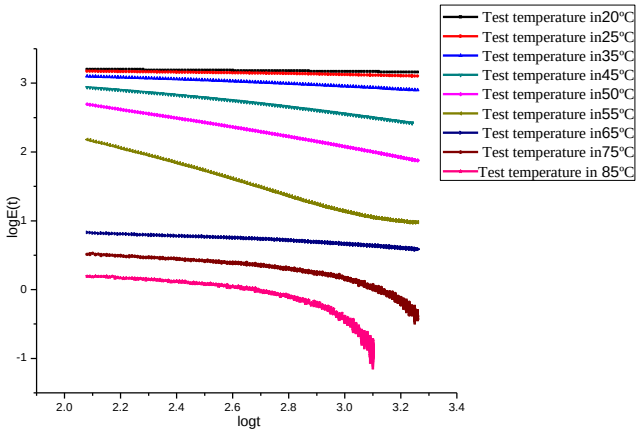

Figure 10 Stress relaxation curves

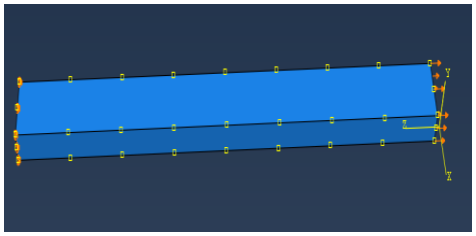

(a) The model used in ABAQUS

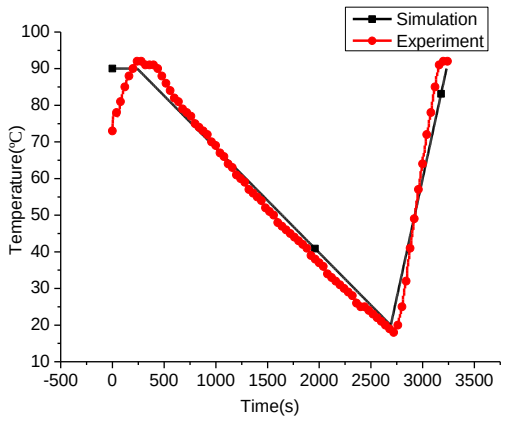

(b) Comparison of temperature-time curves

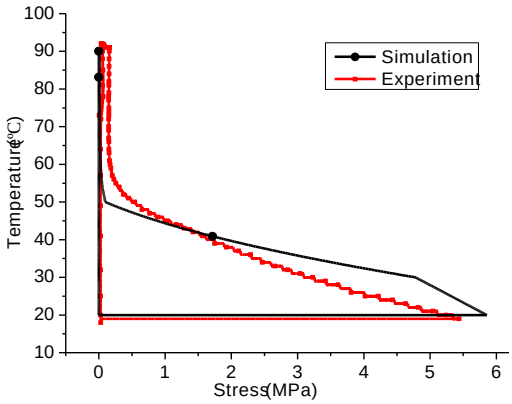

(c) Comparison of stress-temperature curves

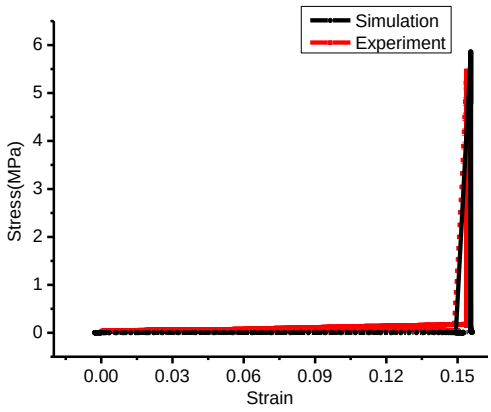

(d) Comparison of stress-strain curves

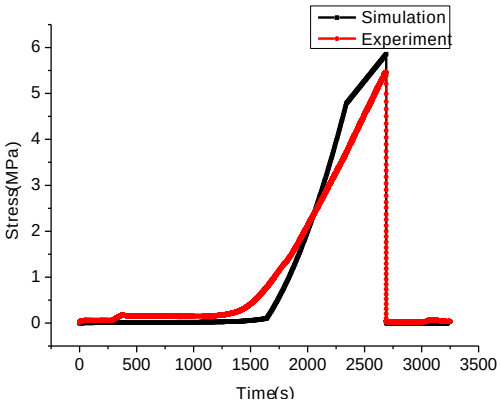

(e) Comparison of Stress-time curves

Figure 11 Simulation of cycle process of SMP

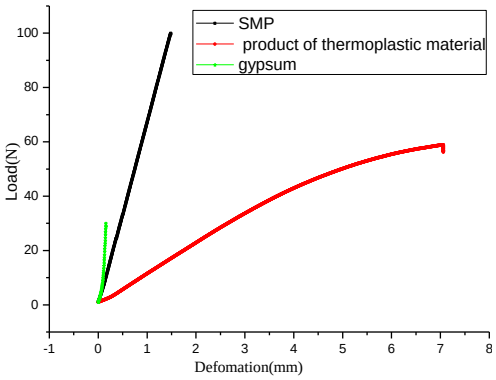

Figure 12 Bending property of SMP, product of thermoplastic material and gypsum

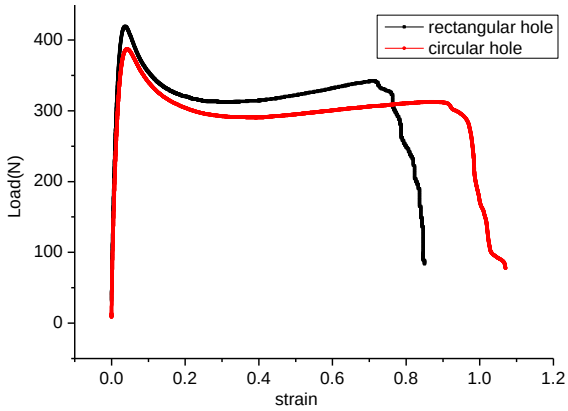

(a) Tension curves of fracture fixator scale model (Deformation rate: 2mm/min)

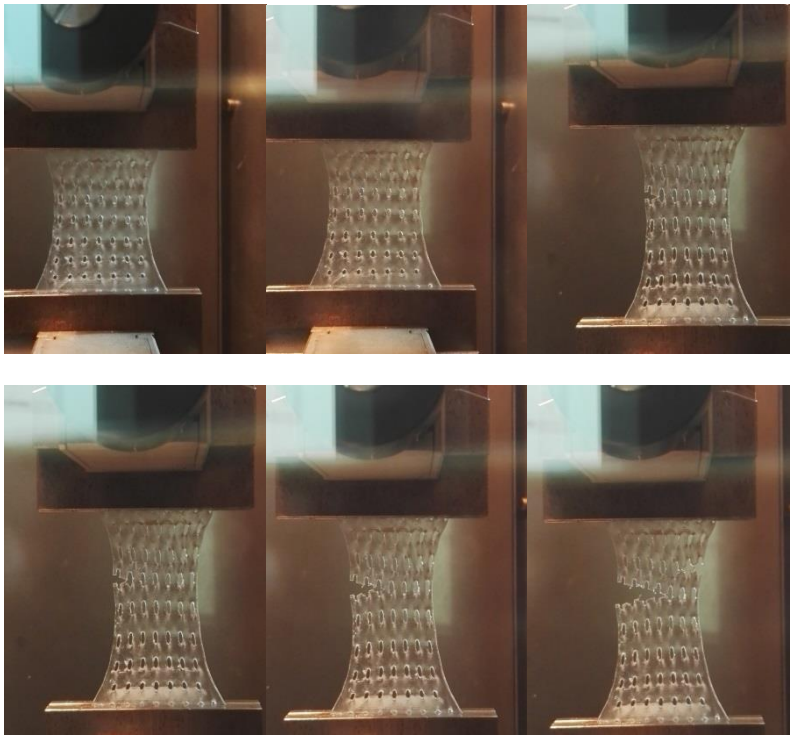

(b) Stretching process of fracture fixator

Figure 13 Tension test of fracture fixator scale model

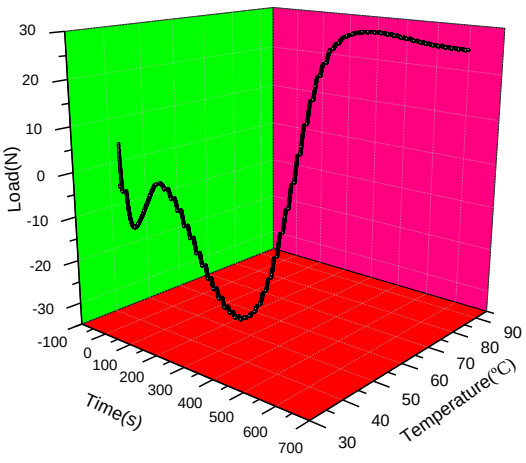

Figure 14 Recover force curve of load-time-temperature

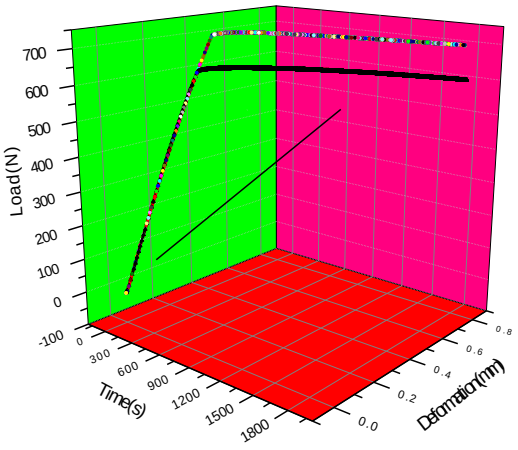

Figure 15 Comparison of creep curves of fracture fixator scale model

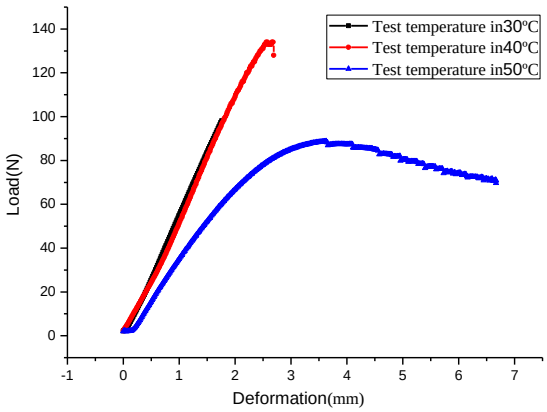

(a) Comparison of three-point bending curves of scale model (Deformation rate: 1mm/min)

(b) Process of three-point bending of fracture fixator at 50°C

Figure 16 Three-point tests of fracture fixator

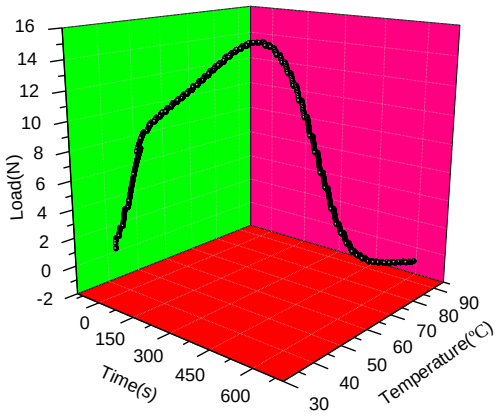

Figure 17 Restoring force curve of 3-point bending test

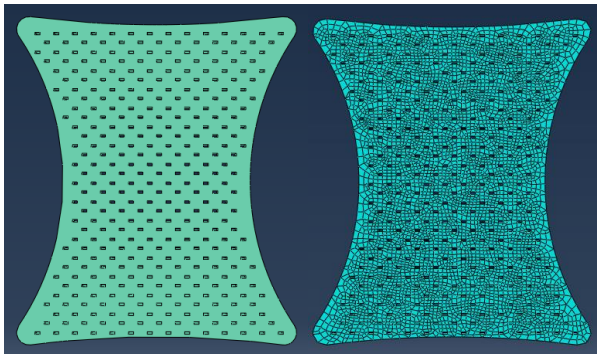

Figure 18 Model of forearm fracture fixator in ABAQUS

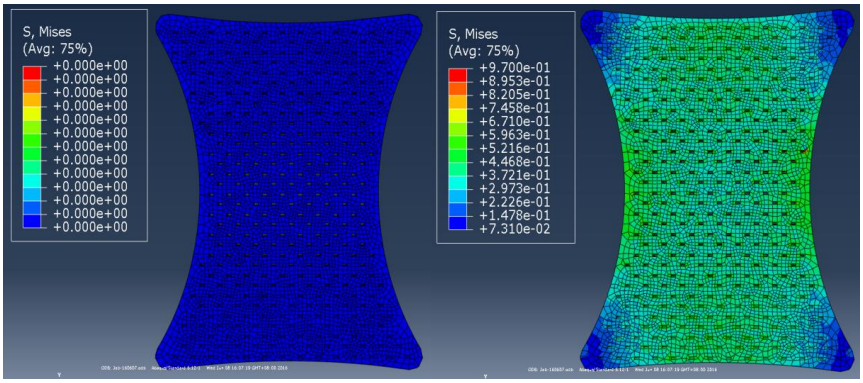

(a) (b)

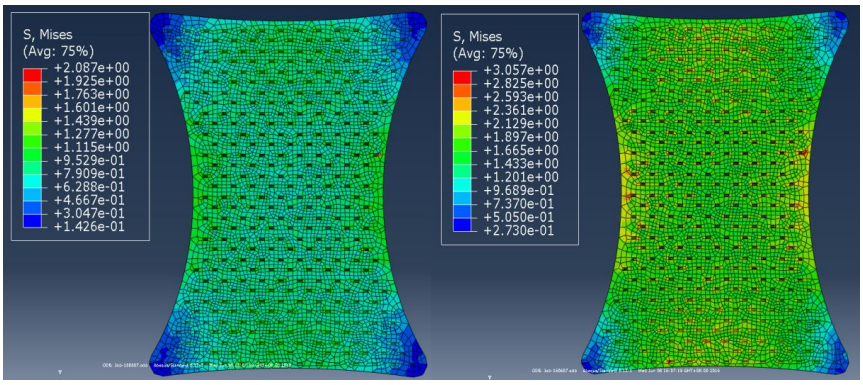

(c) (d)

Figure 19 Stress nephogram of uniaxial tension of fracture fixator (a) stage 1 (b) stage 2 (c) stage 3 (d) stage 4

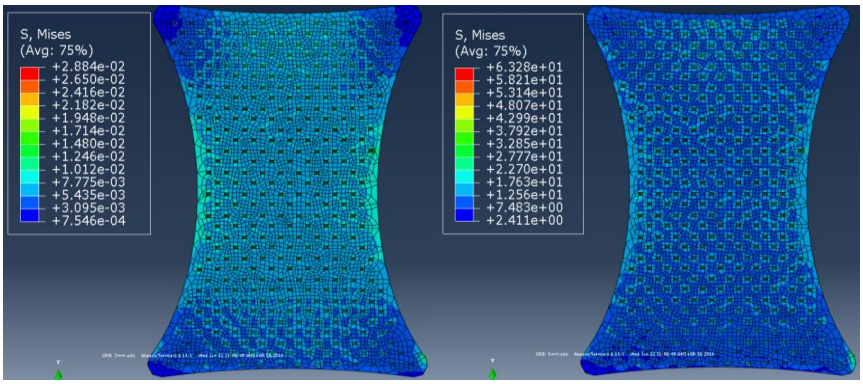

(a) (b)

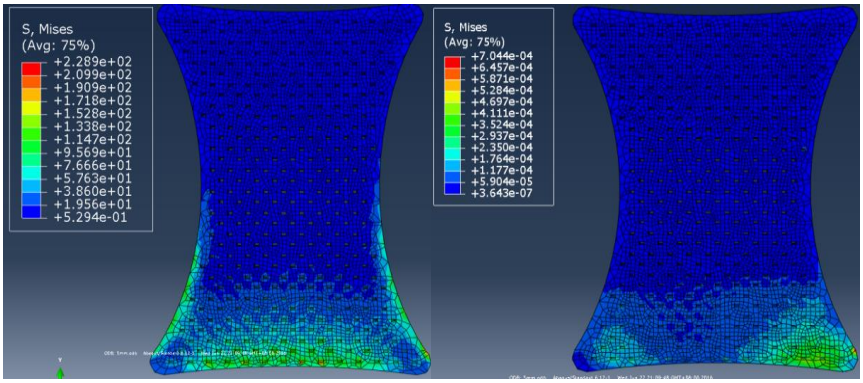

(c) (d)

Figure 20 Stress nephogram of uniaxial tension of fracture fixator (a) step 1 (b) step 2 (c) step 3 (d) step 4

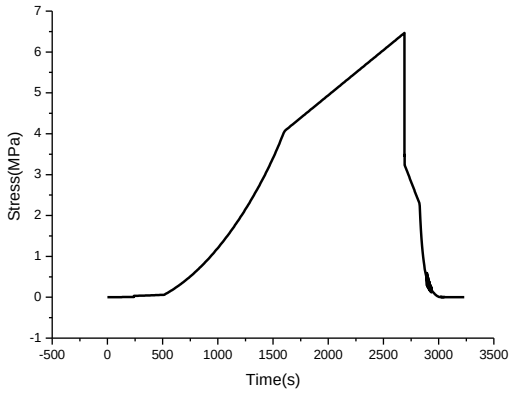

Figure 21 Stress-time curve

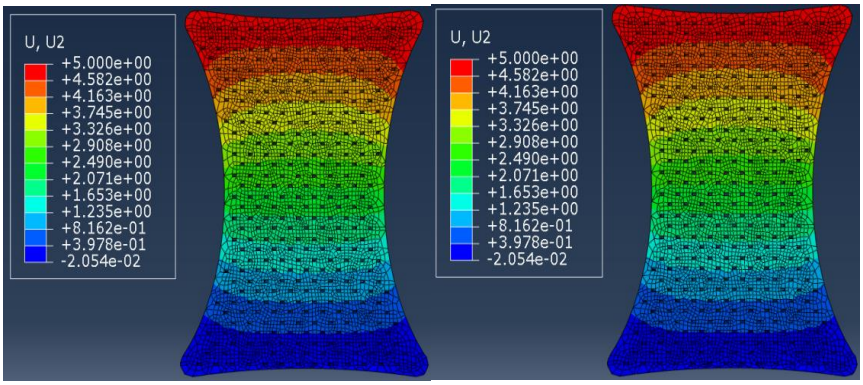

(a) (b)

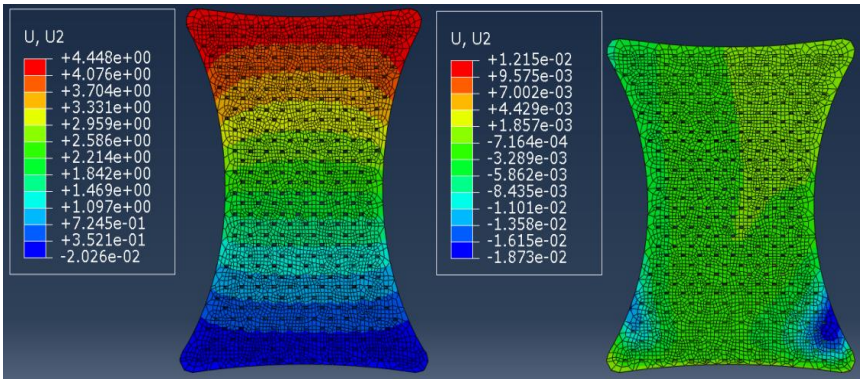

(c) (d)

Figure 22 Displacement fringe of thermomechanical cycle of SMP (a) step 1 (b) step 2 (c) step 3 (d) step 4

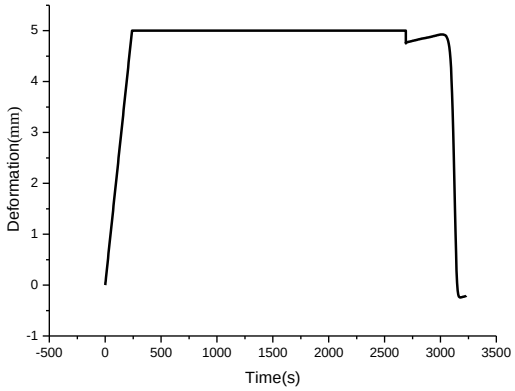

Figure 23 Strain-time curve

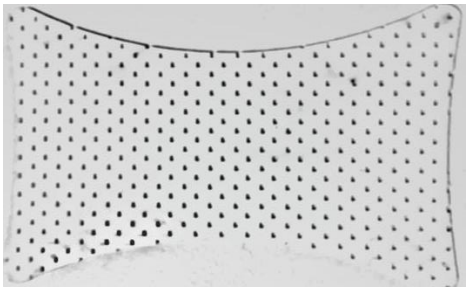

(a) Structure of fixator for arm

(b) Fixing state of arm

Figure 24 Fixator for arm based on SMP

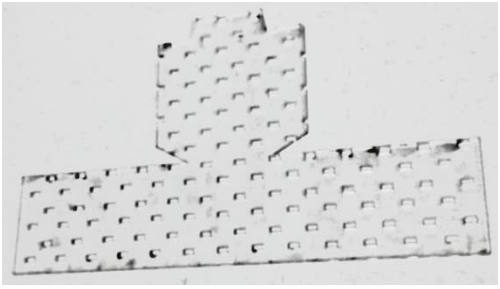

(a) Structure of fixator for middle finger

(b) Fixing state of middle finger

Figure 25 Fixator for middle finger based on SMP

(a) Structure of wrister based on SMP

(b) Fixing state of wrist

Figure 26 Fixator for wrist based on SMP

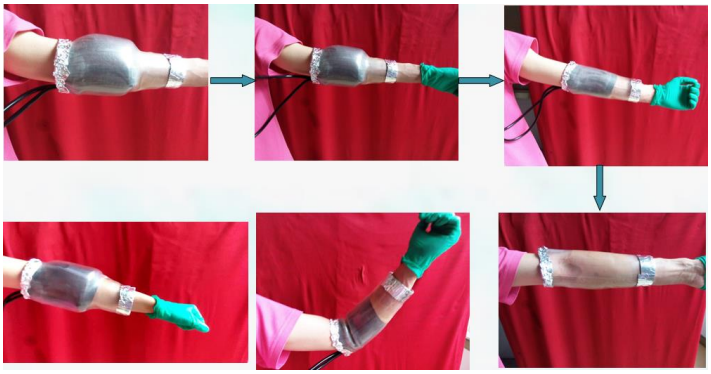

Figure 27 Adaptive fracture Fixator based on SMP

Table 1 Summary of the model parameters of SMP

Description	parameter	values
Viscoelastic parameters	*g1*, *g2*, *g3*, *g4*, *g5*	0.684,0.26,0.049,0.005, 3.6e-4
	τ*1*, τ*2*, τ*3*, τ*4*, τ*5*	1，10,100,1000,10000
Elastic parameters	*E*	125 (at 30°C)
		1.26 (at 55°C)
		0.07 (at 80°C)
Thermal expansion coefficient	a	0.00016 (at 55°C)
WLF reference temperature	*T0*	55°C
WLF constant	*C1*	17.44
WLF constant	C2	51.6